The Astrophysical Journal, 965:159 (11pp), 2024 April 20 https://doi.org/10.3847/1538-4357/ad3440

White Dwarf Merger Remnants: The DAQ Subclass

Mukremin Kilic[1], Pierre Bergeron[2], Simon Blouin[3], Gracyn Jewett[1], Warren R. Brown[4], and Adam Moss[1]
[1] Homer L. Dodge Department of Physics and Astronomy, University of Oklahoma, 440 W. Brooks Street, Norman, OK 73019, USA
[2] Département de Physique, Université de Montréal, C.P. 6128, Succ. Centre-Ville, Montréal, QC, H3C 3J7, Canada
[3] Department of Physics and Astronomy, University of Victoria, Victoria, BC, V8W 2Y2, Canada
[4] Center for Astrophysics, Harvard & Smithsonian, 60 Garden Street, Cambridge, MA 02138, USA
Received 2024 February 21; revised 2024 March 12; accepted 2024 March 13; published 2024 April 17

Abstract

Four years after the discovery of a unique DAQ white dwarf with a hydrogen-dominated and carbon-rich atmosphere, we report the discovery of four new DAQ white dwarfs, including two that were not recognized properly in the literature. We find all five DAQs in a relatively narrow mass and temperature range of $M = 1.14$–$1.19\ M_{\odot}$ and $T_{\rm eff} = 13{,}000$–$17{,}000$ K. In addition, at least two show photometric variations due to rapid rotation with ≈10 minute periods. All five are also kinematically old, but appear photometrically young, with estimated cooling ages of about 1 Gyr based on standard cooling tracks, and their masses are roughly twice the mass of the most common white dwarfs in the solar neighborhood. These characteristics are smoking gun signatures of white dwarf merger remnants. Comparing the DAQ sample with warm DQ white dwarfs, we demonstrate that there is a range of hydrogen abundances among the warm DQ population and that the distinction between DAQ and warm DQ white dwarfs is superficial. We discuss the potential evolutionary channels for the emergence of the DAQ subclass, suggesting that DAQ white dwarfs are trapped on the crystallization sequence and may remain there for a significant fraction of the Hubble time.

Unified Astronomy Thesaurus concepts: White dwarf stars (1799); Atmospheric composition (2120); Stellar evolutionary types (2052); Stellar mergers (2157); DQ stars (1849)

1. Introduction

Short-period double white dwarfs lose angular momentum through gravitational-wave radiation and merge to create a variety of interesting phenomena, including Type Ia supernovae (Iben & Tutukov 1984; Webbink 1984), hot subdwarfs (Heber 2009), R Coronae Borealis stars (Clayton et al. 2007), and ultramassive white dwarfs, or collapse into neutron stars (Nomoto & Iben 1985). Binary population synthesis models demonstrate that the majority of double white dwarf mergers have a combined mass below the Chandrasekhar limit (Toonen et al. 2012). For reference, the field white dwarf mass distribution shows a dominant peak at $0.6\ M_{\odot}$ (Kilic et al. 2020; McCleery et al. 2020). Hence mergers of the most common white dwarfs should form ultramassive white dwarfs with $M \approx 1.2\ M_{\odot}$ (e.g., Kawka et al. 2023).

For the nonexplosive CO + CO white dwarf mergers, the merger remnants experience a luminous giant phase for about 10,000 yr, after which they evolve into single massive white dwarfs with typical rotation periods of 10–20 minutes (Schwab 2021; see also Yoon et al. 2007; Lorén-Aguilar et al. 2009; Shen et al. 2012). Such rotation rates are significantly shorter than the day-long rotation periods seen in pulsating white dwarfs (Kawaler 2015; Hermes et al. 2017), but are now routinely observed in ultramassive and/or magnetic white dwarfs (Kawka 2020; Pshirkov et al. 2020; Caiazzo et al. 2021; Kilic et al. 2021, 2023b; Williams et al. 2022; Moss et al. 2023).

Hot DQ white dwarfs[5] with $T_{\rm eff} \approx 18{,}000$–$24{,}000$ K (Dufour et al. 2008) stand out among the population of rapidly rotating isolated white dwarfs. In addition to fast rotation, hot DQ white dwarfs have high masses $M \geqslant 0.8\ M_{\odot}$, high incidences of magnetism, and unusual kinematics for their age. Even though the emergence of cooler DQ white dwarfs below $T_{\rm eff} = 10{,}000$ K is well explained by the dredging up of carbon in helium-dominated atmospheres (Pelletier et al. 1986; Bédard et al. 2022a), the same dredge-up model fails to explain the chemical composition of warmer DQs (Coutu et al. 2019; Koester & Kepler 2019). Hence, hot DQs must follow a different evolutionary path. All evidence points to a merger origin (Dunlap & Clemens 2015; Coutu et al. 2019; Kawka et al. 2023).

Hollands et al. (2020) reported the discovery of a new spectral class—a DAQ white dwarf with a hydrogen-dominated and carbon-rich atmosphere (WD J055134.612+413531.09, hereafter J0551+4135). Its unusual composition, large mass ($1.14\ M_{\odot}$), and fast kinematics strongly favor a white dwarf merger origin. Large masses, carbon-enriched atmospheres, and fast kinematics are also common characteristics of hot DQ white dwarfs, but it is not clear what causes the unusual atmospheric composition in J0551+4135 or the emergence of the DAQ subclass.

Here we report the discovery of four new DAQ white dwarfs, including three within 100 pc of the Sun. We describe our discovery observations of two new DAQ white dwarfs in Section 2, and present a detailed model atmosphere analysis in Section 3. We present the identification of two additional DAQ white dwarfs that were overlooked in the literature in Section 4, and discuss the distinction between DAQ and DQA white dwarfs in Section 5. We present the physical parameters of the DAQ sample and discuss possible evolutionary channels to explain their unusual compositions in Section 6. We conclude in Section 7.

2. The Discovery of Two New DAQ White Dwarfs

As part of our efforts to constrain the physical properties of the massive white dwarfs in the solar neighborhood

[5] DQ white dwarfs are a spectral class of white dwarfs showing atomic or molecular carbon features (Sion et al. 1983).

Table 1
New DAQ White Dwarfs

Parameter	J0205+2057	J0831−2231	J0958+5853	J2340−1819
Name	G35-26	WDJ083135.57-223133.63	SDSS J095837.00+585303.0	GD 1222
R.A.	02:05:49.45	08:31:35.42	09:58:36.93	23:40:43.98
decl.	+20:57:03.96	−22:31:30.13	+58:53:03.00	−18:19:47.45
Gaia Source ID	94276941624384000	5702793425999272576	1049528378933767424	2393834386459511680
Parallax (mas)	11.712 ± 0.113	12.229 ± 0.081	5.711 ± 0.166	10.582 ± 0.153
$\mu_{\rm R.A.}$ (mas yr^{-1})	−213.07 ± 0.14	−133.22 ± 0.07	−115.14 ± 0.13	−0.58 ± 0.14
$\mu_{\rm decl.}$ (mas yr^{-1})	−250.37 ± 0.11	+218.22 ± 0.08	−9.48 ± 0.17	−114.18 ± 0.10
$V_{\rm tan}$ (km s^{-1})	133.1 ± 1.3	99.1 ± 0.7	95.9 ± 2.8	51.1 ± 0.7

Note. J0205+2057 and J0958+5853 were not properly recognized in the literature.

(G. Jewett et al. 2024, in preparation), we obtained follow-up spectroscopy of $M \geqslant 0.9\ M_{\odot}$ white dwarf candidates in the Montreal White Dwarf Database 100 pc sample (Dufour et al. 2017). To take advantage of the Pan-STARRS photometry in our atmospheric model fits, we further limited our follow-up survey to the Pan-STARRS footprint. We also restricted our sample to objects with $T_{\rm eff} \geqslant 11{,}000$ K, so that helium lines could be detected and used to constrain the atmospheric parameters. Our initial spectroscopic observations at the Apache Point Observatory (APO) 3.5 m telescope revealed two of these candidates, J0831−2231 and J2340−1819 (GD 1222), as potential DAQs. Table 1 presents the photometry and astrometry for these targets.

To confirm their unusual nature, we obtained follow-up spectroscopy of J0831−2231 and J2340−1819 at the 6.5 m MMT on UT 2023 December 9 and 11. We obtained 4×5 minutes back-to-back exposures of each target using the Blue Channel spectrograph (Schmidt et al. 1989), with the 500 l mm^{-1} grating and a 1.″25 slit, providing wavelength coverage 3700–6850 Å and a spectral resolution of 4.7 Å. Hollands et al. (2020) detected low-level 0.4%–0.6% photometric variations in J0551+4135 at a single period of 840 s. In order to search for spectroscopic variations at similar timescales (due to potential changes in the average surface temperature or composition), we also obtained 1 minute long back-to-back exposures of J0551+4135 over 30 minutes on UT 2023 December 8.

Figure 1 shows the combined MMT spectra for J0831−2231 and J2340−1819, along with the DAQ prototype J0551+4135. The dotted lines mark the hydrogen lines; all other observed features are from carbon (Hollands et al. 2020). The striking similarities between the spectra for these three stars confirm that J0831−2231 and J2340−1819 are also DAQ white dwarfs, with spectra dominated by hydrogen lines and secondary features from carbon.

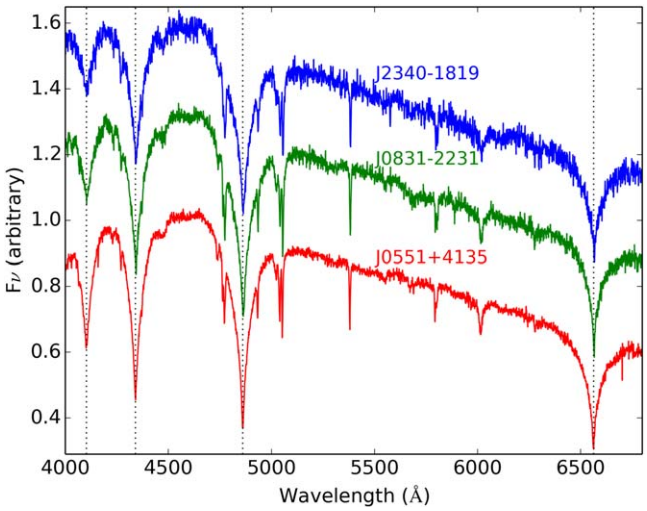

Figure 1. MMT spectra of the newly discovered DAQ white dwarfs J0831−2231 and J2340−1819 compared to the DAQ prototype J0551+4135. The spectra are normalized at 4500 Å and arbitrarily shifted for display purposes. The dotted lines mark the hydrogen Balmer series. All other features are from carbon.

3. Model Atmosphere Analysis

We rely on photometric and spectroscopic techniques (Bergeron et al. 2019) to constrain the physical parameters of our targets. We use Sloan Digital Sky Survey (SDSS) *u* (if available) and Pan-STARRS *grizy* photometry along with Gaia DR3 parallaxes to constrain the effective temperature and the solid angle, $\pi(R/D)^2$, where R is the radius of the star and D is its distance. Since the distance is precisely known from the Gaia parallaxes, we can constrain the radius of the star directly and therefore the mass based on the evolutionary models for white dwarfs. We use the geometric distances from Bailer-Jones et al. (2021) and the reddening values from `STILISM` (Capitanio et al. 2017) for stars beyond 100 pc.

We convert the observed magnitudes into average fluxes using the appropriate zero-points, and compare with the average synthetic fluxes calculated from model atmospheres with the appropriate chemical composition. A χ^2 value is defined in terms of the difference between the observed and model fluxes over all bandpasses, properly weighted by the photometric uncertainties, which is then minimized using the nonlinear least-squares method of Levenberg–Marquardt (Press et al. 1986) to obtain the best-fitting parameters. Given the abundances derived from the spectroscopic fit, we repeat our photometric and spectroscopic fits until a consistent solution is found. The atomic data for carbon are relatively bad, as the oscillator strengths for some of the lines are uncertain by 50% or more. We exclude from our fits the carbon lines with quality flags D and E in the NIST database, and we also exclude two absorption features in the models near 5268 Å and 5668 Å, which are not observed.

For the purpose of this analysis, we rely on two distinct model atmosphere grids based on the calculations of Blouin et al. (2019). The first one, more appropriate for the analysis of DAQ stars, covers the range $T_{\rm eff} = 12{,}000$ K (500 K) 17,000 K, $\log g = 8.0$ (0.5) 9.5, $\rm He/H = 0$, to $\log \rm C/H = -1.5$ (0.5) 2.5 (where the numbers in parentheses indicate the step size). The

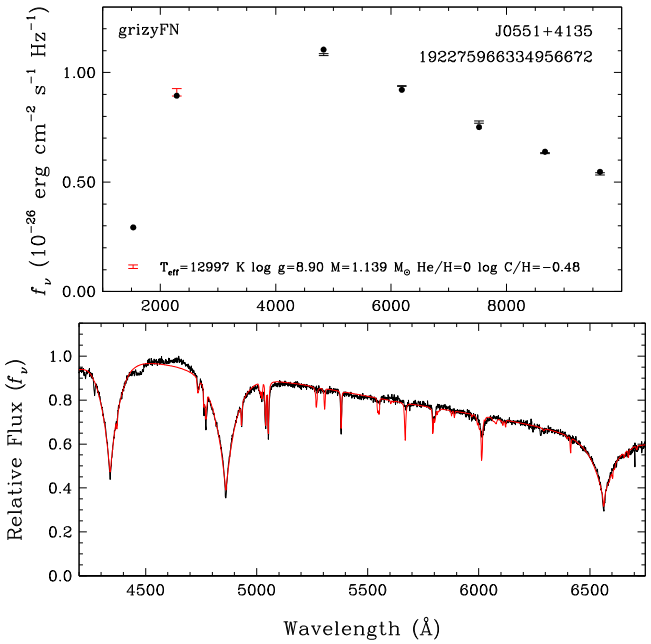

Figure 2. Model atmosphere fits to the previously known DAQ white dwarf J0551+4135. The top and bottom panels show the photometric and spectroscopic fits, respectively. The best-fitting model parameters are presented in the top panel, which also includes the Gaia DR3 Source ID, object name, and the photometry displayed in the panel.

second grid, more appropriate for the analysis of warm DQ/DQA stars, covers the range $T_{\rm eff} = 10{,}000$ K (500 K) 16,000 K, $\log g = 7.0$ (0.5) 9.0, $\log {\rm He/H} = 1.0$ (1.0) 4.0, to $\log {\rm C/He} = -5.0$ (0.5) 1.0.

We rely on the evolutionary models described in Bédard et al. (2020) with CO cores, $q({\rm He}) \equiv \log M_{\rm He}/M_\star = 10^{-2}$, and $q({\rm H}) = 10^{-10}$, which are representative of He-atmosphere (or thin-H-atmosphere) white dwarfs. These evolutionary models are based on single-star evolution, and the assumption of $q({\rm He}) = 10^{-2}$ is likely not representative for merger remnants. However, the helium buffer size has a relatively small effect on the mass–radius relation. For example, for a $T_{\rm eff} = 15{,}000$ K and $M = 1.2\,M_\odot$ star, $\log g$ changes by only 0.003 dex between the evolutionary models with $q({\rm He}) = 10^{-2}$ and 10^{-6}. The helium buffer size also influences the cooling timescales of white dwarfs. However, we show below that our targets are likely delayed in their cooling by billions of years, because of the ^{22}Ne distillation (Blouin et al. 2021; Bédard et al. 2024). Hence, the cooling timescale differences due to a smaller helium buffer are negligible compared to the multi-gigayear cooling delays due the distillation process.

Figure 2 shows our model fits to J0551+4135, the DAQ prototype. The top and bottom panels show our photometric and spectroscopic fits, respectively. The top panel includes GALEX far-UV and near-UV photometry (red error bars; Bianchi et al. 2017) for comparison. The best-fitting model has $T_{\rm eff} = 12{,}997 \pm 115$ K, $\log g = 8.90 \pm 0.01$, $M = 1.139 \pm 0.005\ M_\odot$, and $\log {\rm C/H} = -0.48$. Besides a small flux calibration issue near 4650 Å, this model provides an excellent fit to the observed spectrum, including the Balmer lines and the strongest carbon features. Koester & Kepler (2019) and Hollands et al. (2020) discuss in detail the issues with the accuracy of the oscillator strengths for the carbon lines, especially below 4500 Å. Our best-fitting model underpredicts the carbon line depths in the blue. However, our best-fitting model parameters are consistent with the analysis presented in Hollands et al. (2020), who found $T_{\rm eff} = 13{,}370 \pm 330$ K, $\log g = 8.91 \pm 0.01$, and $\log {\rm C/H} = -0.83$.

A striking feature in J0551+4135's observed spectrum is the flux depression near 4470 Å. Normally, we would associate that feature with the neutral helium line at 4471 Å, which is commonly observed in DB white dwarfs. However, if that feature is really due to He I, then we should also see a stronger He I absorption feature at 5876 Å, which is clearly absent. We explored model atmospheres with varying helium abundances, and found that it is impossible to have a strong 4471 Å feature and hide the one at 5876 Å. Hollands et al. (2020) gave an upper limit of $\log {\rm He/H} < -0.3$ based on the absence of the latter. They also associate the feature around 4470 Å with carbon, though there was a typo in their paper and this feature was erroneously reported as 4570 Å (M. Hollands 2024, private communication). Unfortunately, there are significant uncertainties in the oscillator strengths for the carbon lines in the blue; for example, Koester & Kepler (2019) find factor of ∼4 differences between the NIST, VALD, and literature values for the C I λ4270.221 Å line. Hence, we are not able to resolve the issue with the 4470 Å feature at this point, but it is clearly not from He I, and is most likely from the carbon triplet at 4467.714 Å, 4478.727 Å, and 4479.840 Å (vacuum). Regardless of these issues with matching the carbon lines below about 4500 Å, we confirm that J0551+4135 has a hydrogen-dominated atmosphere with significant amounts of carbon present, and that there is no evidence of any helium in its spectrum.

Figure 3 shows our model fits to the newly discovered DAQ white dwarfs J0831−2231 and J2340−1819. Even though the problems in matching some of the carbon lines persist, as in J0551+4135, carbon and hydrogen atmosphere models provide an excellent match to the overall spectra of both targets. Table 2 presents the best-fitting model parameters for each source. These two stars are slightly hotter and even more carbon-rich than J0551+4135, but otherwise they have similar masses and estimated cooling ages of ∼1 Gyr. As discussed above, these ages are based on standard single-star evolution and are likely strongly underestimated.

4. Two Additional DAQ White Dwarfs Hiding in the Literature

The discovery of two new DAQs in our follow-up sample (G. Jewett et al. 2024, in preparation) prompted us to revisit the spectral classification of warm DQ white dwarfs. Through this process, we identified two additional DAQ white dwarfs that were not properly recognized in the literature: J0205+2057 (G35-26) and J0958+5853 (SDSS J095837.00+585303.0).

Liebert (1983) identified J0205+2057 as the first white dwarf to show atomic lines of both hydrogen and carbon, classifying it as a DAQ3 white dwarf in the spectral classification system of Sion et al. (1983). He noted that it is tempting to identify this star with the hot end of the helium-rich white dwarfs that show traces of dredged-up carbon (DQ type), but his search for the He I λ5876 Å line was unsuccessful. Based on a model atmosphere analysis, Thejll et al. (1990) concluded that J0205+2057 has a helium-dominated atmosphere with a temperature between 11,000 and 14,000 K and a hydrogen abundance of 0.5%–1% by number. However, this analysis was based on a blue spectrum that did not include the

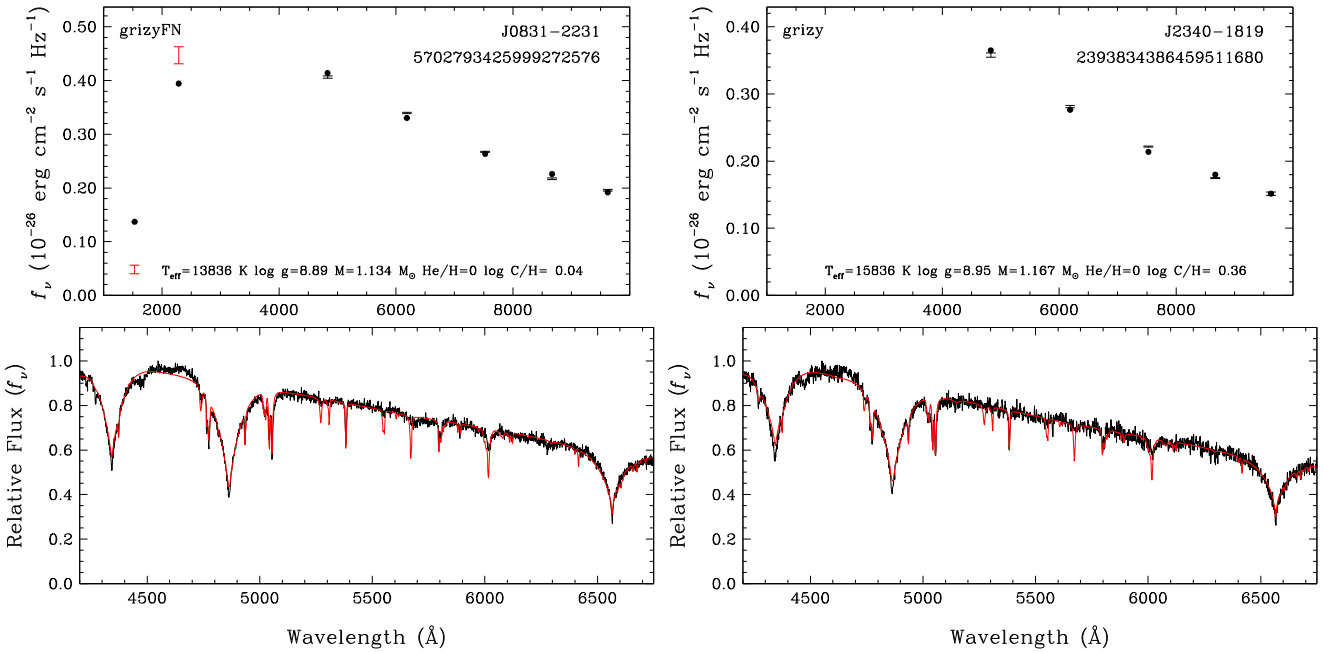

Figure 3. Model atmosphere fits to two newly discovered DAQ white dwarfs. The symbols are the same as in Figure 2.

He I λ5876 Å line, and they erroneously associated the broad feature at 4470 Å with He I.

Figure 4 shows the optical photometry and spectroscopy of J0205+2057 along with our model atmosphere fits under the assumption of a helium-dominated atmosphere (log H/He = − 2). First of all, the spectral classification of white dwarfs solely depends on the observed spectrum (Sion et al. 1983) and not the composition determined from a model atmosphere analysis. Here, the Balmer lines are the strongest features, and the carbon lines are secondary. Hence, J0205 +2057 is clearly a DAQ white dwarf, and as Liebert (1983) noted, it is the first DAQ white dwarf ever found. Second, given the severe problems with the atomic data for carbon (see, e.g., Koester & Kepler 2019), the broad feature from carbon lines near 4470 Å is easily confused with the He I feature at 4471 Å, leading to incorrect atmospheric composition measurements. Our spectroscopic model fit under the assumption of a helium-dominated atmosphere provides a decent fit to the observed 4470 Å feature, but it predicts an even stronger helium feature at 5876 Å that is clearly not observed. The He I λ5876 Å feature is the strongest feature in DB white dwarfs, and it is the last helium feature to disappear (see, for example, the infamous case of GD 362 in Zuckerman et al. 2007).

Figure 5 shows the carbon and hydrogen atmosphere model fits for J0205+2057 and another DAQ overlooked in the literature, J0958+5853. Both of these stars have Balmer lines that are stronger than the carbon lines, hence are clearly DAQ white dwarfs. Here, the DAQ models provide an excellent match to the spectra of both targets, and all of the arguments presented here for J0205+2057 also apply to the spectrum of J0958+5853. Besides the obvious problems with matching some of the carbon lines, as in the other DAQs discussed above, the Balmer lines and the carbon features are fit fairly well by models with log C/H ≈ 0.9. Adding J0205+2057 and J0958+5853 to the list, we now have a class of DAQ white dwarfs with at least five members, four of which are in the 100 pc sample.

5. The Distinction between DAQ and DQA White Dwarfs

Many of the warm DQ white dwarfs show evidence of hydrogen in their spectra (Coutu et al. 2019; Koester & Kepler 2019), and several of them display relatively strong Hα and Hβ lines. Figure 6 shows the spectral energy distributions and our model fits for two such objects. The spectra for these two stars appear relatively similar to the DAQ stars discussed above. However, we found it difficult to classify these objects: the carbon lines are slightly deeper than the Hβ line, but it is hard to tell if they are also deeper than the Hα line. These stars were classified either as DQ or DQA in the literature (Kepler et al. 2015; Coutu et al. 2019).

Traditionally, warm DQ and DQA white dwarfs are expected to have helium-dominated atmospheres. However, we now know that the broad feature at 4470 Å is not from helium and it is most likely due to carbon, as none of these stars display the much stronger He I λ5876 line. Analyzing the spectral energy distributions of warm DQs with parallax measurements under the assumption of helium-dominated atmospheres, Koester & Kepler (2019) found that they could constrain the C/He ratio in these atmospheres relatively well, as long as log C/He $\leqslant -1$. However, at higher ratios, the errors become as large as 0.7 dex. In addition, in two cases, including J1448+0519 shown here, their best-fit models with helium-dominated models predict strong helium lines that are not observed (see their Figure 1). They could not constrain the abundances for those two stars, but they were able to put an upper limit on the He/C ratio from the absence of He I λ5876. However, given the lack of any helium lines in the spectra of these stars, it is also possible to fit warm DQA stars with no helium, as we did for the DAQ stars.

Figure 6 shows the results from this experiment for these two DQA white dwarfs. Carbon and hydrogen atmosphere models provide fits that are just as good as the fits using the carbon and helium (and trace amounts of hydrogen) atmospheres. The spectral energy distributions of these two stars can be explained by models with $T_{\rm eff}$ = 15,000–16,000 K and log C/H ranging

Table 2
Physical Parameters for the DAQ White Dwarfs

Parameter	J0205+2057	J0551+4135	J0831−2231	J0958+5853	J2340−1819
$T_{\rm eff}$ (K)	16,427 ± 228	12,997 ± 115	13,836 ± 180	16,871 ± 478	15,836 ± 291
log g	9.01 ± 0.02	8.90 ± 0.01	8.89 ± 0.01	8.99 ± 0.04	8.95 ± 0.02
Mass ($M_\odot$)	1.194 ± 0.008	1.139 ± 0.005	1.134 ± 0.007	1.184 ± 0.019	1.167 ± 0.011
log C/H	+0.97	−0.48	+0.04	+0.91	+0.36
Cooling age[1] (Gyr)	0.96 ± 0.04	1.44 ± 0.03	1.23 ± 0.04	0.88 ± 0.08	0.97 ± 0.05

Note. (1) Based on single-star evolution and assuming CO cores. These cooling ages are most likely strongly underestimated compared to the true ages.

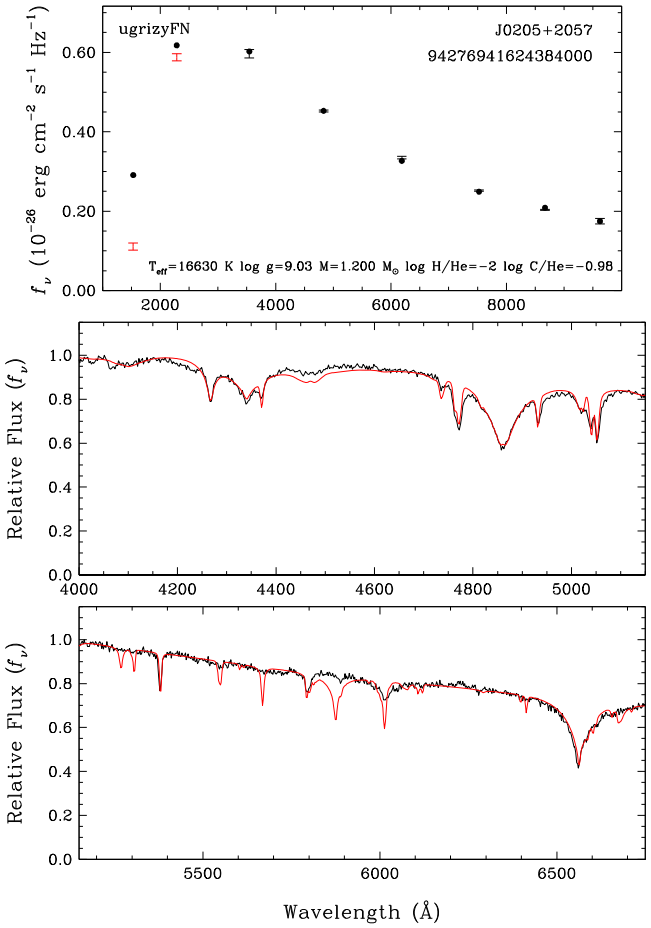

Figure 4. Model atmosphere fits to J0205+2057 under the assumption of a helium-dominated atmosphere. Note the relatively strong He I λ5876 Å feature predicted in the models that is not observed in the spectrum of this object in the bottom panel. This indicates that J0205+2057 does not have a helium-dominated atmosphere. In fact, there is no evidence of helium in the spectrum of this DAQ white dwarf.

from +1.01 to +1.19. These parameters are similar to the temperatures derived for the DAQ white dwarfs discussed above, and the C/H ratios are slightly higher. Note that we are not claiming that these DQA white dwarfs have no helium; we simply cannot tell if there is any. Due to the absence of helium features in their spectra, we can at best put an upper limit on the He/C ratio, but this ratio could be as low as zero.

Figure 7 shows the H/C ratio for the warm DQ white dwarfs from Koester & Kepler (2019) and Coutu et al. (2019), as well as the 100 pc sample of G. Jewett et al. (2024, in preparation), under the assumption of carbon and hydrogen atmospheres with no helium. We restrict this plot to the temperature and abundance ranges covered by our DAQ model grid. Note that the assumption of a helium-free atmosphere has minimal impact on the derived H/C ratios for these stars, since no helium lines are observed. For reference, the helium-dominated and helium-free model fits shown in Figures 4 and 5 for J0205+2057 have log H/C = −1.02 and −0.97, respectively.

Figure 7 shows that DAQ white dwarfs are the most hydrogen-rich stars among the warm DQ sample, but otherwise they belong to the same population. Regardless of whether there is helium or not in the atmosphere, this figure demonstrates that the distinction between DAQ and DQA white dwarfs is superficial; warm DQ white dwarfs simply display a range of hydrogen abundances in their atmospheres, and depending on how much hydrogen is present and which lines are stronger, we classify them as a DAQ, DQA, or DQ.

6. Discussion

6.1. Kinematics

Hollands et al. (2020) noted the unusual kinematics of J0551+4135 for its cooling age. J0551+4135 has a tangential velocity of only 30 km s^{-1}. However, including its gravitational-redshift-corrected radial velocity of −114 km s^{-1}, its total velocity with respect to the local standard of rest is 129 ± 5 km s^{-1}. The remaining four DAQs have larger tangential velocities (see Table 1): all have $V_{\rm tan} \geqslant 51$ km s^{-1}, and three have $V_{\rm tan} \geqslant 96$ km s^{-1}, pointing to a kinematically old thick-disk or halo population.

We measure radial velocities of −2.8 ± 12.6, 142.1 ± 18.9, and 128.8 ± 20.0 km s^{-1} from our MMT spectra for J0551+4135, J0831−2231, and J2340−1819, respectively. The former is consistent with the radial velocity measurement (before the gravitational redshift correction) of +2.7 ± 5.1 km s^{-1} from Hollands et al. (2020). We measure radial velocities of −18.3 ± 41.9 and 203.2 ± 21.4 km s^{-1} for J0205+2057 and J0958+5853, respectively, using their SDSS spectra. Given the relatively large masses of these white dwarfs and the gravitational redshift corrections of ≈120 km s^{-1}, J0205+2057, J0551+4135, and J0958+5853 have a relatively large line-of-sight motion.

We compute the *UVW* velocities using the Gaia parallax and zero-point correction, and we correct the values to the local standard of rest (Schönrich et al. 2010). Table 3 presents these velocities. Four of the DAQs orbit with the Sun ($|V| \leqslant 31$ km s^{-1}) and all five have small vertical velocities ($|W| \leqslant 21$ km s^{-1}). However, the *U* components of motion (toward/away from the Galactic center) for these stars are relatively large. J0205+2057 is moving toward the Galactic center at 198 ± 27 km s^{-1} and J0551+4135 at 130 ± 12 km s^{-1}, whereas J0958+5853 is going in the opposite direction at −109 ± 13 km s^{-1}. Figure 8 plots the distribution of Galactic *U*, *V*, and *W* velocity components for our five targets, along with the 1σ (dotted) and 2σ (dashed) velocity ellipsoids for the thick disk and halo (Chiba & Beers 2000). J0205

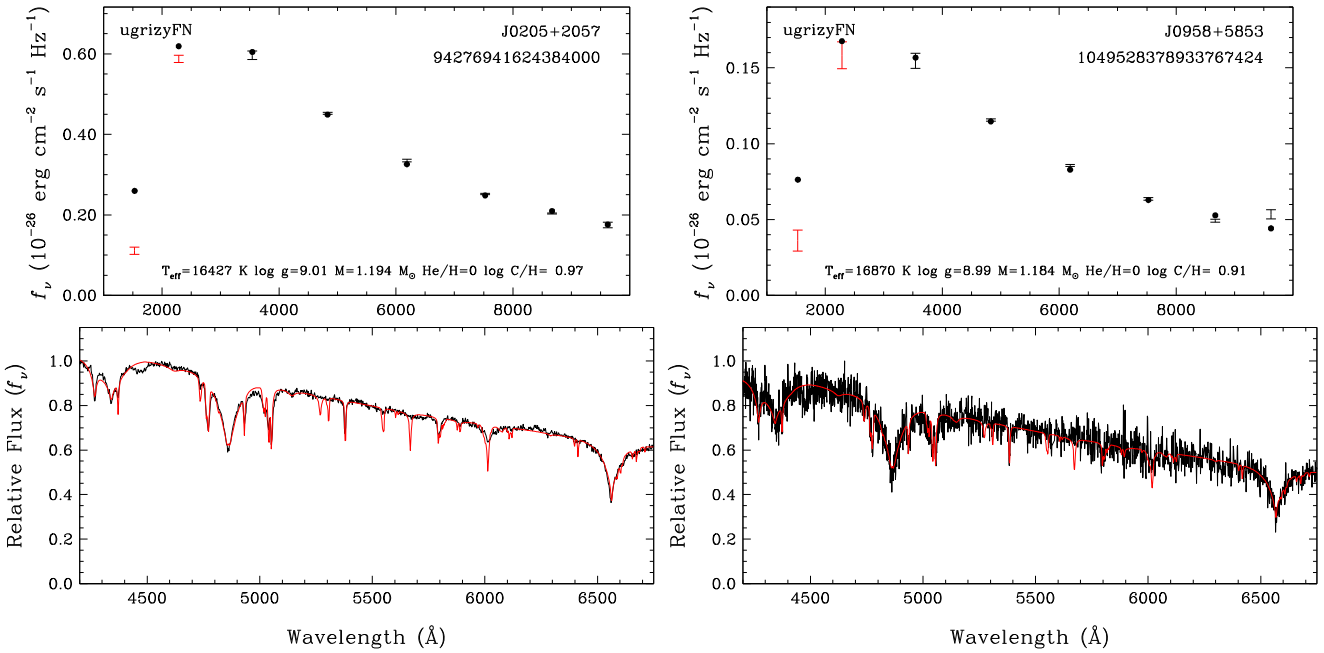

Figure 5. Mixed carbon and hydrogen atmosphere model fits to two DAQ white dwarfs that were not properly recognized in the literature.

+2057 is likely a halo member, whereas J0831−2231, J0958 +5853, and J2340−1819 are likely thick-disk objects. J0551 +4135 is more ambiguous, but its small V and W velocities suggest it is probably a thick-disk object as well; it is only 46 pc away. Clearly, these five DAQs belong to a kinematically old population, even though their estimated cooling ages are of order 1 Gyr under the assumption of single-star evolution.

6.2. Rapid Rotation in J0831−2231 and J2340−1819

We acquired high-speed photometry of three of the DAQs—J0205+2057, J0831−2231, and J2340−1819—on UT 2023 December 23, December 30, and 2024 February 9 using the APO 3.5 m telescope with the Astrophysical Research Consortium Telescope Imaging Camera (ARCTIC) and the BG40 filter. We obtained back-to-back exposures of 10 s over $\geqslant$2 hr for each target. We binned the CCD by 3 × 3, which resulted in a plate scale of $0\farcs34$ pixel^{-1} over a field of view of 7.85 square arcmin. This setup results in an overhead of 4.5 s for each exposure, resulting in a cadence of 14.5 s.

Figure 9 shows the APO light curves and their Fourier transforms. There is no evidence of short-term variability in J0205+2057's light curve (top left) at the 4⟨A⟩ level, where ⟨A⟩ is the average amplitude in the Fourier transform. However, the other two stars presented in this figure are clearly variable. The bottom left panels show the light curve of J0831−2231 obtained over 3 hr on 2023 December 30, along with its Fourier transform. There is only a single significant peak detected at a frequency of $1560.6 \pm 3.5\,\mu$ Hz with 14.1 ± 1.0 millimodulation amplitude (mma). J0831−2231 is outside of the ZZ Ceti instability strip. In addition, since only a single mode is detected, the variability must be due to rotation along with either a spotted surface or an inhomogeneous atmosphere. Regardless of the exact cause of variability, J0831 −2231 is rotating with a period of only 10.7 minutes.

The right panels in Figure 9 show the APO light curves of J2340−1819 from two different nights separated by a week. The light curves cover 120 and 116 minutes, respectively. There is only a single significant peak detected on 2023 December 23 at a frequency of $1383.8 \pm 10.6\,\mu$Hz with an amplitude of 9.3 ± 1.3 mma. The data from 2023 December 30 also show a single significant frequency at $1378.9 \pm 3.8\,\mu$Hz, with an amplitude of 15.7 ± 0.7 mma and its first harmonic at a frequency of $2764.7 \pm 11.0\,\mu$Hz. J2340−1819 is clearly outside of the ZZ Ceti instability strip, and rotates rapidly with a period of 12 minutes.

J0551+4135 is the only DAQ within the boundaries of the ZZ Ceti instability strip (see Figure 4 in Kilic et al. 2023a). Carbon does not affect the excitation of g modes in DAQ white dwarfs, since the excitation is due to the κ mechanism by the dominant chemical species—in this case, hydrogen (A. Córsico 2024, private communication). Both Vincent et al. (2020) and Hollands et al. (2020) reported the discovery of pulsations in J0551+4135 with a single frequency peak. The latter obtained time-series photometry over several nights, and found that this single peak changed both in frequency (from 1186 to 1202 μHz) and amplitude (by a factor of 2) over a 10 day period. This change in frequency is possible for pulsations, but not for rotation. Hollands et al. (2020) suggest that the change in amplitude could be due to unresolved rotational splitting.

Our time-series spectroscopy obtained over 30 minutes for J0551+4135 does not provide any additional constraints on the rotation period. Fitting each 1 minute long spectroscopic exposure, we find that the log (C/H) ratio of the best-fitting model to the spectra ranges from −0.54 to −0.44, with an average of -0.48 ± 0.02 dex. We obtained additional time-series photometry of J0551+4135 at the APO 3.5 m telescope and detected multimode pulsations over a few nights. However, the number of detected modes is still relatively small, and it does not enable us to perform detailed asteroseismology of this object yet. Hence, the rotation periods of J0551+4135 and J0958+5853 remain currently unconstrained.

6.3. The Origin of the DAQ Class

Hollands et al. (2020) proposed carbon dredge-up as the source of the DAQ phenomenon. They suggest that the mixed

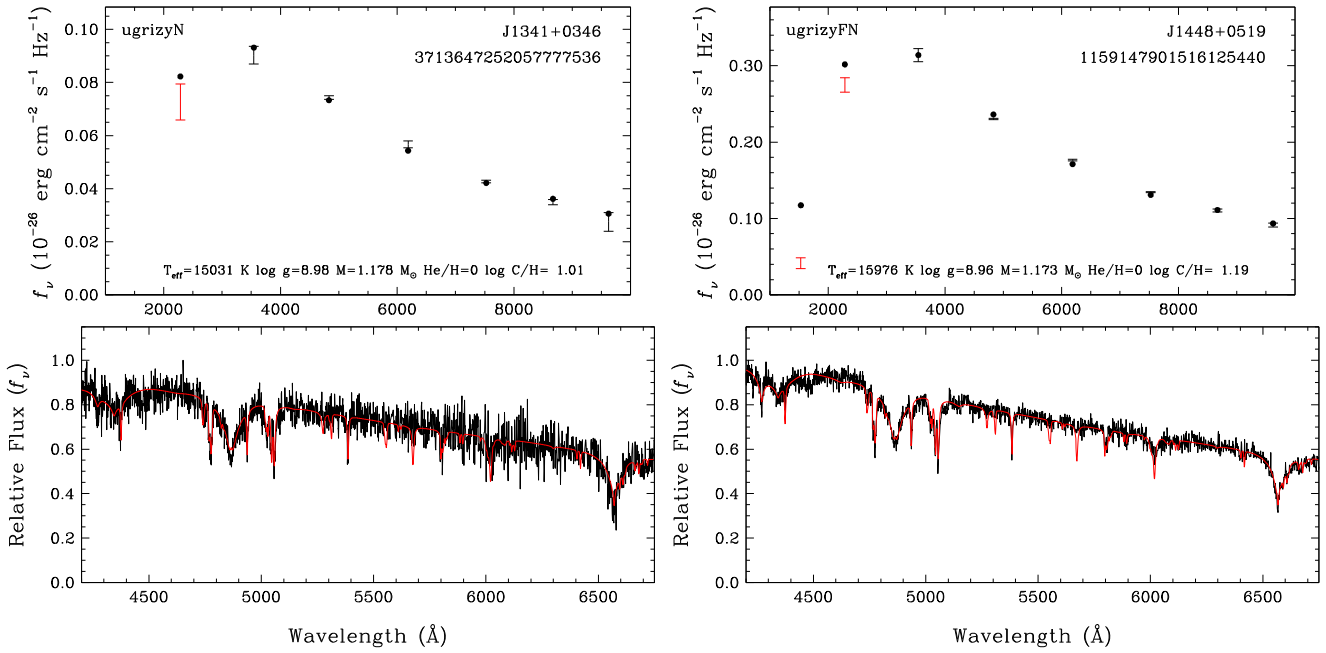

Figure 6. Examples of carbon and hydrogen atmosphere model fits to two warm DQA white dwarfs with strong Balmer lines. These objects are J1341+0346 (SDSS J134124.28+034628.7) and J1448+0519 (WD 1446+055).

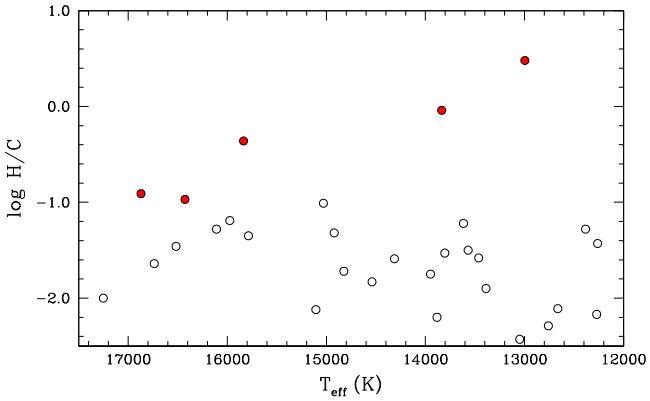

Figure 7. H/C ratio vs. effective temperature for warm DQ white dwarfs. The red points mark the five DAQ white dwarfs identified here.

Table 3
UVW Velocities for the DAQ Sample

Object	U (km s^{-1})	V (km s^{-1})	W (km s^{-1})
J0205+2057	198 ± 27	-64 ± 19	4 ± 26
J0551+4135	130 ± 12	-8 ± 2	21 ± 2
J0831−2231	-89 ± 8	31 ± 17	18 ± 3
J0958+5853	-109 ± 13	14 ± 7	4 ± 16
J2340−1819	35 ± 3	-31 ± 5	-5 ± 19

hydrogen and carbon atmosphere of J0551+4135 can be explained if both hydrogen and helium masses are significantly lower than expected from single-star evolution. For low helium masses, the helium layer diffuses downward, creating a hydrogen/carbon interface and enabling carbon dredge-up into the hydrogen envelope. Before we discuss potential evolutionary scenarios for the emergence of the DAQ subclass, we first summarize observations relevant to this discussion.

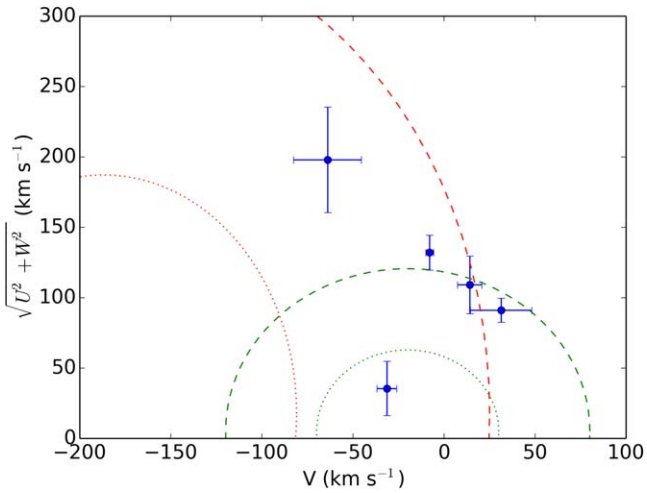

Figure 8. Toomre diagram for the DAQ white dwarf sample. The dotted and dashed lines show the 1σ and 2σ velocity ellipsoids for the thick disk (green) and halo (red lines), respectively (Chiba & Beers 2000).

Observations of the five DAQ white dwarfs identified in this study indicate that they display many similarities with the hot DQ and warm DQ populations: they are massive, have carbon-enriched atmospheres, display unusual kinematics for their cooling ages, and (at least two out of five) display photometric variability due to fast rotation.

Figure 10 summarizes the stellar masses as a function of effective temperature for the five DAQ white dwarfs presented in this paper, along with the Montreal White Dwarf Database 100 pc sample (Kilic et al. 2020), as well as the hot DQ and warm DQ white dwarfs taken from the samples of Coutu et al. (2019), Koester & Kepler (2019), and G. Jewett et al. (2024, in preparation). All warm DQs in this figure have been reanalyzed using the same technique as described above, but assuming an almost undetectable trace of helium of $\mathrm{He/C} = 1$.

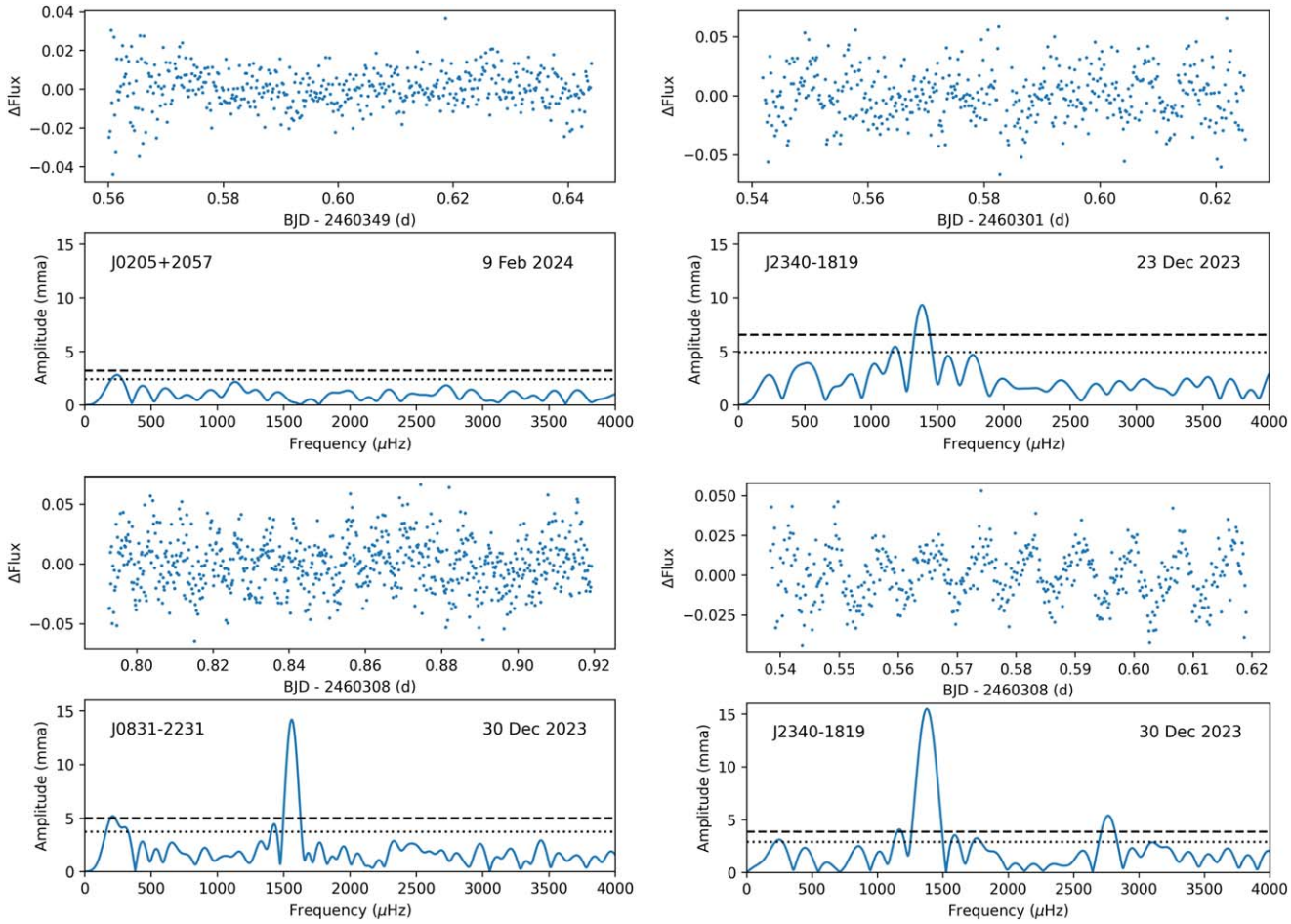

Figure 9. APO time-series photometry of three DAQ white dwarfs (top panels) and their Fourier transforms (bottom panels). The dotted and dashed lines show the $3\langle A\rangle$ and $4\langle A\rangle$ levels. J2340−1819 was observed on two different nights (right panels).

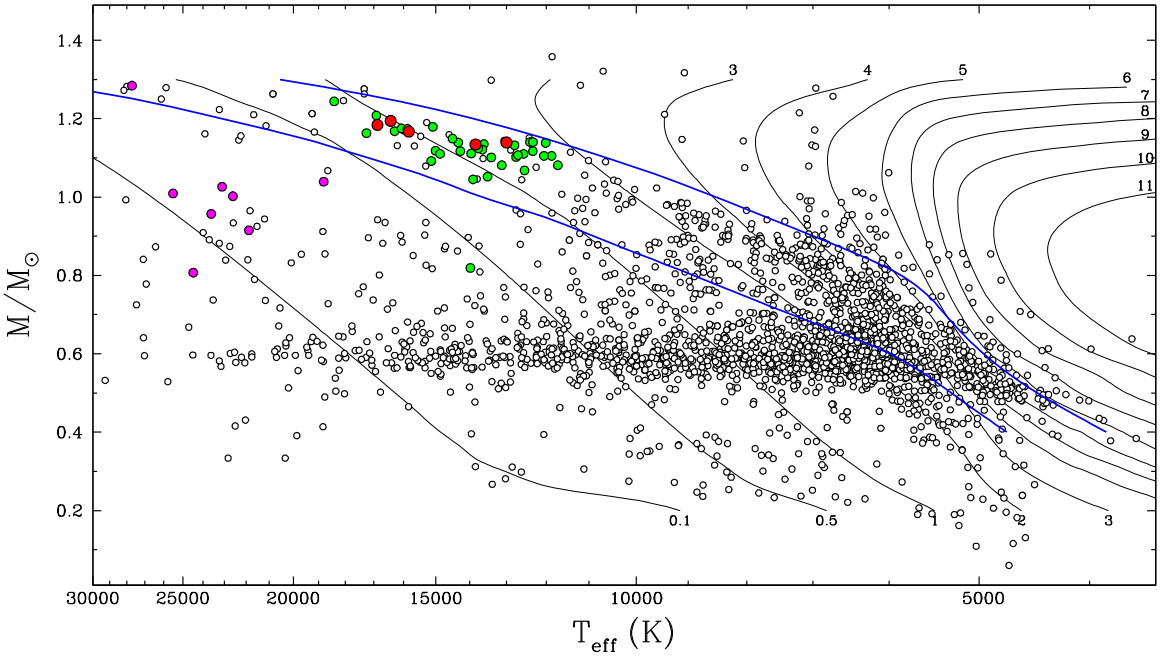

Figure 10. Stellar masses as a function of effective temperature for the Montreal White Dwarf Database 100 pc sample (white dots), along with the hot DQ (magenta) and warm DQ (green) white dwarfs. The red dots mark the five DAQs identified in this paper. The solid curves are theoretical isochrones, labeled in units of gigayears, obtained from standard cooling sequences with CO-core compositions, $q(\mathrm{He}) \equiv M(\mathrm{He})/M_\star = 10^{-2}$, and $q(\mathrm{H}) = 10^{-4}$. The lower blue solid curve indicates the onset of crystallization at the center of the evolving models, while the upper one indicates the locations where 80% of the total mass has solidified.

We can see that hot DQ white dwarfs are prevalent above $T_{\rm eff} = 18{,}000$ K, while the DAQ subclass emerges below about 17,000 K. The seven hot DQs analyzed by Koester & Kepler (2019) have masses ranging from 0.81 to 1.04 $M_{\odot}$, and they are found outside of the CO crystallization branch. More importantly, they have masses lower than those of the DAQ white dwarfs, and hence they are unlikely progenitors of the DAQ spectral class, unless the masses of these hot DQ stars are significantly underestimated. However, J1819−1208 (Kilic et al. 2023b), the only hot DQ in the 100 pc sample, is much more massive and is also located within the crystallization sequence.

Interestingly, all DAQ white dwarfs and all but one of the warm DQ white dwarfs displayed in Figure 10 lie within the crystallization boundary, and none are cooler. The only exception is the warm DQ SDSS J104052.40+063519.7, with a mass near 0.8 $M_{\odot}$. Coutu et al. (2019) note that J1040+0635 is magnetic, but further observations are needed to understand the unusual nature of this object and to see if its relatively low inferred mass could be due to binarity.

Excluding J1040+0635, all of the DAQ and warm DQ stars share the same parameter space in the M versus $T_{\rm eff}$ diagram, suggesting that they have a common origin. The main difference between the DAQs and warm DQs is the amount of hydrogen they contain, as previously shown in Figure 7. Indeed, many of the warm DQs contain significant amounts of hydrogen (Dufour et al. 2008; Koester & Kepler 2019), and a few of the hot DQs as well. For example, Dufour et al. (2008) identified two hot DQ white dwarfs with $T_{\rm eff} \sim 21{,}000$ K and with visible Hβ lines that indicate log C/H ≈ 1.7. This is similar to the C/H ratios measured in warm DQs (see Figure 7).

Cheng et al. (2019) identified a cooling anomaly of high-mass white dwarfs on the crystallization sequence of CO white dwarfs (the so-called Q-branch; Gaia Collaboration et al. 2018; Tremblay et al. 2019) and found that 5%–9% of the high-mass white dwarfs experience an extra cooling delay of at least 8 Gyr that cannot be accounted for by standard core crystallization or merger delays.

Blouin et al. (2021) suggested that a phase separation process involving ^{22}Ne (not to be confused with the gravitational settling of ^{22}Ne in the liquid phase) might generate enough energy to produce a multigigayear pause in the cooling of CO white dwarfs. For typical CO-core compositions, it has been shown that the solid phase is depleted in ^{22}Ne compared to the liquid. This can lead to the creation of buoyant crystals that inhibit the standard inside-out crystallization scenario. The buoyant crystals float up and thereby displace ^{22}Ne-rich liquid toward the center of the star in a solid–liquid distillation process that liberates copious amounts of gravitational energy (Isern et al. 1991). This has now been implemented in white dwarf cooling models and been shown to match all the observational properties of Q-branch white dwarfs (Bédard et al. 2024). The exact origin of these delayed Q-branch objects remains unclear.

The facts that the Q-branch coincides with CO crystallization and that the distillation mechanism requires CO cores suggest that these white dwarfs must harbor CO cores. This is in tension with the predictions from Schwab (2021), who find that for ultramassive white dwarfs with masses exceeding 1.05 $M_{\odot}$, both single-star evolution and the merger of two CO white dwarfs should yield an ONe white dwarf. However, Dominguez et al. (1996) demonstrated that during the CO-core formation, even a small initial rotation may have a significant impact on the evolutionary outcome. The decrease in core pressure, brought on by the anticipated increase in angular velocities during the compression of the CO core at the onset of the asymptotic giant branch (AGB) phase, leads to a reduction in maximum temperature. This favors the formation of ultramassive CO white dwarfs with masses exceeding 1.05 $M_{\odot}$. Furthermore, Althaus et al. (2021) have more recently corroborated this phenomenon through detailed computations of single progenitor evolution, confirming the formation of ultramassive CO white dwarfs.

A possible progenitor channel for the delayed Q-branch population is the merger of white dwarfs and subgiant stars, which can produce the ultramassive CO white dwarfs with enough neutron-rich impurities needed to power the distillation mechanism (Shen et al. 2023). Given that DAQ and warm DQ stars are likely merger remnants, have old kinematic ages, and are confined to the crystallization sequence (Figure 10), it is natural to assume that they are currently undergoing a distillation-powered multigigayear cooling pause. Indeed, Cheng et al. (2019) find that half of the extra delayed population is made of DQ stars. Hence, we end up with the interesting idea that the spectral evolution of DAQ and warm DQ white dwarfs may proceed at nearly constant effective temperature. We explore below the possibilities that DAQ stars evolve into warm DQ white dwarfs and the other way around.

6.4. Evolutionary Path of DAQs

In the temperature range where warm DQ stars are found ($T_{\rm eff} \sim 13{,}000$–$17{,}000$ K), their atmospheres and stellar envelopes are strongly convective, even more so at large masses (see, e.g., Figures 9 and 10 of Rolland et al. 2020). This is certainly the case for DAQ white dwarfs as well, otherwise they would not have mixed hydrogen and carbon compositions. Hence it is not possible for hydrogen to float to the surface through ordinary diffusion, a process that requires the environment to be convectively stable. It is thus very unlikely that warm DQ/DQA white dwarfs evolve into DAQ stars.

A more likely scenario is that DAQ white dwarfs evolve into warm DQ stars through a process analogous to one of the most well-established spectral evolution scenarios, namely the DO → DA → DB/DC transformation (Bédard et al. 2022a). In this scenario, a hot, helium-atmosphere DO star evolves over time into a DA white dwarf, when hydrogen starts floating toward the surface as a result of ordinary diffusion in a radiative envelope. In this particular context, stratified DAO stars are believed to be transitional objects. As evolution proceeds, some of these DA stars with thin enough hydrogen layers will be convectively diluted near 20,000 K and become DBA white dwarfs (objects with thicker hydrogen layers may be convectively mixed below about 12,000 K and become helium-rich DA stars or DC white dwarfs). Based on detailed calculations of the spectral evolution of white dwarfs (Bédard et al. 2022b), including different chemical transport mechanisms, Bédard et al. (2023) also predict the existence of a massive hydrogen reservoir underneath the thin superficial layer, and demonstrate that the atmospheric hydrogen in DBA stars is likely from this internal reservoir of residual hydrogen (see also Rolland et al. 2020). This model successfully reproduces the observed H/He ratios among DBA white dwarfs, which comprise as much as 60%–75% of the DB

population in the solar neighborhood (Koester & Kepler 2015; Rolland et al. 2018). Hydrogen always remains a trace element, however, in the sense that DBA white dwarfs never become DA white dwarfs at lower temperatures.

We are likely witnessing a similar phenomenon in the DAQ and warm DQ sample, but with a very different interior, with carbon being much closer to the surface than normal post-AGB objects, likely as a result of the merger process. In this proposed scenario, a thin hydrogen atmosphere (in a hot massive DA star) is being diluted by the deeper C/He-rich convective envelope as the star cools off, gradually turning this massive DA white dwarf into a DAQ and eventually into a warm DQA star, as hydrogen is being diluted further within the deep C/He convective envelope.

Because these massive white dwarfs are trapped on the crystallization sequence, they go through the DA to DQA spectral evolution at a relatively constant surface temperature. The amount of hydrogen in warm DQA stars is most likely too high for a simple dilution process, and a deep hydrogen reservoir may also be required, as in DBA white dwarfs (Rolland et al. 2020; Bédard et al. 2023).

In this scenario, the immediate progenitors of DAQ stars are probably massive DA white dwarfs with extremely thin hydrogen layers, although carbon enrichment seems to be a rare phenomenon among the relatively young, ultramassive DA white dwarf population. However, it is also possible that the even more distant progenitors are massive, hot DQ stars, such as J1819−1208 (see Figure 10), in which the residual hydrogen present in the radiative envelope eventually floats to the surface through ordinary diffusion. If the total hydrogen mass is too small, these hot DQ stars may evolve directly into warm DQs or DQAs, without becoming DAQ white dwarfs. A similar situation occurs in the context of DB white dwarfs, where hot DO stars may evolve directly into DB or DBA white dwarfs, without ever becoming DA stars, if the total mass of hydrogen is too small (Bédard et al. 2023). Althaus et al. (2005) highlighted the impact of the internal diffusion of diluted hydrogen during the born-again phase on the formation of white dwarfs, and demonstrated the evolutionary connection between PG1159-DB-DC/DQ white dwarfs.

To summarize, we propose two potential evolutionary channels involving warm DQ and DAQ white dwarfs. Depending on how much hydrogen is present in the stellar envelope, the white dwarf merger remnant may appear as a massive DA or a hot DQ. The proposed channels are:

1) DA → DAQ → warm DQA; and
2) Hot DQ(A) → warm DQ(A).

In the second scenario, hot DQs may evolve into warm DQs where hydrogen is either not seen or has trace amounts in the atmosphere.

In both of our proposed evolutionary scenarios, the stars are trapped on the crystallization sequence. This would explain why we do not observe their cooler counterparts (massive, cool DQ white dwarfs) in the solar neighborhood (see, e.g., Kilic et al. 2020; Caron et al. 2023). Detailed evolutionary calculations for the spectral evolution of hot and warm DQs are currently not available, but would be helpful in further understanding the emergence of the DAQ subclass.

7. Conclusions

Through follow-up spectroscopy of massive white dwarf candidates within 100 pc, we have identified two new DAQ white dwarfs with mixed carbon and hydrogen atmospheres. In addition, based on a detailed model atmosphere analysis, we have demonstrated that two additional DAQ white dwarfs were overlooked in the literature. These four objects increase the sample of DAQ white dwarfs from one (Hollands et al. 2020) to five.

The DAQ white dwarf sample shows several characteristics that favor a merger origin. All five stars have masses in the range 1.14–1.19 $M_{\odot}$, roughly twice the average mass for the DA white dwarfs in the solar neighborhood. In addition, all five are relatively young, with cooling ages of about 1 Gyr, but kinematically old, with tangential velocities greater than 50 km s^{-1} and as high as 133 km s^{-1}. Their Galactic UVW velocities point to a thick-disk or halo origin. In addition, we detect rapid rotation in at least two of these objects. These characteristics are all very similar to the warm DQ white dwarf population, which also lies within the crystallization sequence.

Given the similarities between the warm DQ population and the DAQ white dwarfs discovered here, we propose two potential evolutionary channels for DAQ and warm DQ stars. The DAQ population likely emerges as massive DA white dwarfs, produced in white dwarf mergers, are convectively mixed. Shen et al. (2023) propose subgiant + CO white dwarf mergers as the progenitors of a significant fraction of the Q-branch white dwarfs with delayed cooling times. Further theoretical studies of the spectral evolutions of merger products, including hot and warm DQs and the DAQs, would be beneficial for understanding the emergence of the DAQ subclass.

Acknowledgments

We are grateful to Antoine Bédard for useful discussions. This work is supported in part by the NSF under grant AST-2205736, NASA under grants 80NSSC22K0479, 80NSSC24K0380, and 80NSSC24K0436, NSERC Canada, the Fund FRQ-NT (Québec), the Canadian Institute for Theoretical Astrophysics (CITA) National Fellowship Program, and the Smithsonian Institution.

Based on observations obtained at the MMT Observatory, a joint facility of the Smithsonian Institution and the University of Arizona.

The Apache Point Observatory 3.5 m telescope is owned and operated by the Astrophysical Research Consortium.

Facilities: MMT (Blue Channel spectrograph), ARC (KOSMOS spectrograph, ARCTIC imager).

ORCID iDs

Mukremin Kilic https://orcid.org/0000-0001-6098-2235
Pierre Bergeron https://orcid.org/0000-0003-2368-345X
Simon Blouin https://orcid.org/0000-0002-9632-1436
Gracyn Jewett https://orcid.org/0009-0009-9105-7865
Warren R. Brown https://orcid.org/0000-0002-4462-2341
Adam Moss https://orcid.org/0000-0001-7143-0890

References

Althaus, L. G., Gil-Pons, P., Córsico, A. H., et al. 2021, A&A, 646, A30
Althaus, L. G., Serenelli, A. M., Panei, J. A., et al. 2005, A&A, 435, 631
Bailer-Jones, C. A. L., Rybizki, J., Fouesneau, M., et al. 2021, AJ, 161, 147
Bédard, A., Bergeron, P., Brassard, P., et al. 2020, ApJ, 901, 93
Bédard, A., Bergeron, P., & Brassard, P. 2022a, ApJ, 930, 8
Bédard, A., Bergeron, P., & Brassard, P. 2023, ApJ, 946, 24
Bédard, A., Blouin, S., & Cheng, S. 2024, Natur, 627, 286
Bédard, A., Brassard, P., Bergeron, P., et al. 2022b, ApJ, 927, 128
Bergeron, P., Dufour, P., Fontaine, G., et al. 2019, ApJ, 876, 67

Bianchi, L., Shiao, B., & Thilker, D. 2017, ApJS, 230, 24
Blouin, S., Daligault, J., & Saumon, D. 2021, ApJL, 911, L5
Blouin, S., Dufour, P., Thibeault, C., & Allard, N. F. 2019, ApJ, 878, 63
Caiazzo, I., Burdge, K. B., Fuller, J., et al. 2021, Natur, 595, 39
Capitanio, L., Lallement, R., Vergely, J. L., et al. 2017, A&A, 606, A65
Caron, A., Bergeron, P., Blouin, S., et al. 2023, MNRAS, 519, 4529
Cheng, S., Cummings, J. D., & Ménard, B. 2019, ApJ, 886, 100
Chiba, M., & Beers, T. C. 2000, AJ, 119, 2843
Clayton, G. C., Geballe, T. R., Herwig, F., Fryer, C., & Asplund, M. 2007, ApJ, 662, 1220
Coutu, S., Dufour, P., Bergeron, P., et al. 2019, ApJ, 885, 74
Dominguez, I., Straniero, O., Tornambe, A., et al. 1996, ApJ, 472, 783
Dufour, P., Blouin, S., Coutu, S., et al. 2017, in ASP Conf. Ser. 509, 20th European White Dwarf Workshop, ed. P. E. Tremblay, B. Gaensicke, & T. Marsh (San Francisco, CA: ASP), 3
Dufour, P., Fontaine, G., Liebert, J., Schmidt, G. D., & Behara, N. 2008, ApJ, 683, 978
Dunlap, B. H., & Clemens, J. C. 2015, in ASP Conf. Ser. 493, 19th European Workshop on White Dwarfs, ed. P. Dufour, P. Bergeron, & G. Fontaine (San Francisco, CA: ASP), 547
Gaia Collaboration, Babusiaux, C., van Leeuwen, F., et al. 2018, A&A, 616, A10
Heber, U. 2009, ARA&A, 47, 211
Hermes, J. J., Gänsicke, B. T., Kawaler, S. D., et al. 2017, ApJS, 232, 23
Hollands, M. A., Tremblay, P. E., Gänsicke, B. T., et al. 2020, NatAs, 4, 663
Iben, I. J., & Tutukov, A. V. 1984, ApJS, 54, 335
Isern, J., Hernanz, M., Mochkovitch, R., et al. 1991, A&A, 241, L29
Kawaler, S. D. 2015, in ASP Conf. Ser. 493, 19th European Workshop on White Dwarfs, ed. P. Dufour, P. Bergeron, & G. Fontaine (San Francisco, CA: ASP), 65
Kawka, A. 2020, in IAU Symp. 357, White Dwarfs as Probes of Fundamental Physics: Tracers of Planetary, Stellar and Galactic Evolution, ed. M. A. Barstow et al. (Cambridge: Cambridge Univ. Press), 60
Kawka, A., Ferrario, L., & Vennes, S. 2023, MNRAS, 520, 6299
Kepler, S. O., Pelisoli, I., Koester, D., et al. 2015, MNRAS, 446, 4078
Kilic, M., Bergeron, P., Kosakowski, A., et al. 2020, ApJ, 898, 84
Kilic, M., Córsico, A. H., Moss, A. G., et al. 2023a, MNRAS, 522, 2181
Kilic, M., Kosakowski, A., Moss, A. G., Bergeron, P., & Conly, A. A. 2021, ApJL, 923, L6
Kilic, M., Moss, A. G., Kosakowski, A., et al. 2023b, MNRAS, 518, 2341
Koester, D., & Kepler, S. O. 2015, A&A, 583, A86
Koester, D., & Kepler, S. O. 2019, A&A, 628, A102
Liebert, J. 1983, PASP, 95, 878
Lorén-Aguilar, P., Isern, J., & García-Berro, E. 2009, A&A, 500, 1193
McCleery, J., Tremblay, P.-E., Gentile Fusillo, N. P., et al. 2020, MNRAS, 499, 1890
Moss, A., Kilic, M., Bergeron, P., Firgard, M., & Brown, W. 2023, MNRAS, 523, 5598
Nomoto, K., & Iben, I. 1985, ApJ, 297, 531
Pelletier, C., Fontaine, G., Wesemael, F., Michaud, G., & Wegner, G. 1986, ApJ, 307, 242
Press, W. H., Flannery, B. P., & Teukolsky, S. A. 1986, Numerical Recipes: The Art of Scientific Computing (Cambridge: Cambridge Univ. Press)
Pshirkov, M. S., Dodin, A. V., Belinski, A. A., et al. 2020, MNRAS, 499, L21
Rolland, B., Bergeron, P., & Fontaine, G. 2018, ApJ, 857, 56
Rolland, B., Bergeron, P., & Fontaine, G. 2020, ApJ, 889, 87
Schmidt, G. D., Weymann, R. J., & Foltz, C. B. 1989, PASP, 101, 713
Schönrich, R., Binney, J., & Dehnen, W. 2010, MNRAS, 403, 1829
Schwab, J. 2021, ApJ, 906, 53
Shen, K. J., Bildsten, L., Kasen, D., & Quataert, E. 2012, ApJ, 748, 35
Shen, K. J., Blouin, S., & Breivik, K. 2023, ApJL, 955, L33
Sion, E. M., Greenstein, J. L., Landstreet, J. D., et al. 1983, ApJ, 269, 253
Thejll, P., Shipman, H. L., MacDonald, J., & Macfarland, W. M. 1990, ApJ, 361, 197
Toonen, S., Nelemans, G., & Portegies Zwart, S. 2012, A&A, 546, A70
Tremblay, P.-E., Fontaine, G., Fusillo, N. P. G., et al. 2019, Natur, 565, 202
Vincent, O., Bergeron, P., & Lafrenière, D. 2020, AJ, 160, 252
Webbink, R. F. 1984, ApJ, 277, 355
Williams, K. A., Hermes, J. J., & Vanderbosch, Z. P. 2022, AJ, 164, 131
Yoon, S. C., Podsiadlowski, P., & Rosswog, S. 2007, MNRAS, 380, 933
Zuckerman, B., Koester, D., Melis, C., Hansen, B. M., & Jura, M. 2007, ApJ, 671, 872